



**HAL**  
open science

## The interplay of geology, climate and tectonics on river incision: the example of the High Verdon Gorges, Southwestern French Alps

Thibaut Cardinal, Carole Petit, Yann Rolland, Stéphane Schwartz, Pierre Gaston Valla, Bruno Scalabrino, Laurence Audin, Maxime Bertauts, Swann Zerathe, Denis Thiéblemont, et al.

### ► To cite this version:

Thibaut Cardinal, Carole Petit, Yann Rolland, Stéphane Schwartz, Pierre Gaston Valla, et al.. The interplay of geology, climate and tectonics on river incision: the example of the High Verdon Gorges, Southwestern French Alps. *Comptes Rendus. Géoscience*, 2024, 356 (S2), pp.265-287. 10.5802/cr-geos.216 . hal-04229416

**HAL Id: hal-04229416**

**<https://hal.science/hal-04229416v1>**

Submitted on 5 Oct 2023

**HAL** is a multi-disciplinary open access archive for the deposit and dissemination of scientific research documents, whether they are published or not. The documents may come from teaching and research institutions in France or abroad, or from public or private research centers.

L'archive ouverte pluridisciplinaire **HAL**, est destinée au dépôt et à la diffusion de documents scientifiques de niveau recherche, publiés ou non, émanant des établissements d'enseignement et de recherche français ou étrangers, des laboratoires publics ou privés.



INSTITUT DE FRANCE  
Académie des sciences

# *Comptes Rendus*

---

## *Géoscience*

### *Sciences de la Planète*

Thibaut Cardinal, Carole Petit, Yann Rolland, Stéphane Schwartz, Pierre Gaston Valla, Bruno Scalabrino, Laurence Audin, Maxime Bertauts, Swann Zerathe, Denis Thiéblemont, Régis Braucher and ASTER Team

**The interplay of geology, climate and tectonics on river incision: the example of the High Verdon Gorges, Southwestern French Alps**

Published online: 25 July 2023

<https://doi.org/10.5802/crgeos.216>

**Part of Special Issue:** Geodynamics of Continents and Oceans – A tribute to Jean Aubouin

**Guest editors:** Olivier Fabbri (Université de Franche-Comté, UMR CNRS 6249, Besançon), Michel Faure (Université d'Orléans-BRGM, UMR CNRS 7325, Institut des Sciences de la Terre, Orléans), Laurent Jolivet (Sorbonne Université, ISTeP, UMR 7193, Paris) and Sylvie Leroy (Sorbonne Université, CNRS-INSU, ISTeP, Paris)



This article is licensed under the  
CREATIVE COMMONS ATTRIBUTION 4.0 INTERNATIONAL LICENSE.  
<http://creativecommons.org/licenses/by/4.0/>



*Les Comptes Rendus. Géoscience — Sciences de la Planète sont membres du  
Centre Mersenne pour l'édition scientifique ouverte*

[www.centre-mersenne.org](http://www.centre-mersenne.org)

e-ISSN : 1778-7025



---

Geodynamics of Continents and Oceans – A tribute to Jean Aubouin

# The interplay of geology, climate and tectonics on river incision: the example of the High Verdon Gorges, Southwestern French Alps

Thibaut Cardinal<sup>\*, a</sup>, Carole Petit<sup>® a</sup>, Yann Rolland<sup>® b, c</sup>, Stéphane Schwartz<sup>® b</sup>, Pierre Gaston Valla<sup>® b</sup>, Bruno Scalabrino<sup>a</sup>, Laurence Audin<sup>® b</sup>, Maxime Bertauts<sup>b</sup>, Swann Zerathe<sup>® b</sup>, Denis Thiéblemont<sup>® d</sup>, Régis Braucher<sup>e</sup> and ASTER Team<sup>e, f</sup>

<sup>a</sup> Université Côte d'Azur, CNRS, Observatoire de la Côte d'Azur, IRD, Géoazur, 250 rue Albert Einstein, Sophia Antipolis 06560 Valbonne, France

<sup>b</sup> Université Grenoble Alpes, Université Savoie Mont Blanc, CNRS, IRD, Université Gustave Eiffel, ISTerre, 38000 Grenoble, France

<sup>c</sup> Université Savoie Mont Blanc, CNRS, Pôle Montagne, Edytem, F-73370 Le Bourget-du-Lac, France

<sup>d</sup> DGR/CGEO, BRGM, B.P. 6009, 45060 Orléans, Cedex, France

<sup>e</sup> Université Aix-Marseille, CNRS-IRD-Collège de France-INRAE, UM 34 CEREGE, Technopôle de l'Environnement Arbois-Méditerranée, BP80, 13545 Aix-en-Provence, France

<sup>f</sup> ASTER Team: Georges Aumaître, Didier L. Bourlès<sup>†</sup>, Karim Keddadouche

*E-mails:* cardinal@geoazur.unice.fr (T. Cardinal), petit@geoazur.unice.fr (C. Petit), yann.rolland@univ-smb.fr (Y. Rolland), stephane.schwartz@univ-grenoble-alpes.fr (S. Schwartz), pierre.valla@univ-grenoble-alpes.fr (P. G. Valla), Bruno.SCALABRINO@geoazur.unice.fr (B. Scalabrino), laurence.audin@ird.fr (L. Audin), maxime.bertauts@univ-grenoble-alpes.fr (M. Bertauts), swann.zerathe@ird.fr (S. Zerathe), d.thieblemont@brgm.fr (D. Thiéblemont), braucher@cerge.fr (R. Braucher)

**Abstract.** Deciphering the impact of short-term or long-term forcing on fluvial incision, as well as understanding the influence of local (channel lithology and morphology) and global (tectonic motions) parameters in the spatial variation of incision efficiency, are ongoing geomorphological research fields. To shed new light on these issues, we chose to study the “Hautes Gorges du Verdon” (High Verdon Gorges or HVG), located in the foreland of the Southwestern Alps. We collected 24 samples along three polished surfaces for Cosmic Ray Exposure (CRE) <sup>36</sup>Cl dating, which allowed us to constrain short-term incision rates ranging from 0.06 to 0.2 mm/yr between 60 and 15 ka. Compared to known regional uplift and denudation rates, incision rates obtained in the HVG suggest tectonic or isostatic uplift as the main driver of Verdon River incision in the Late Quaternary. This comparison allows us to propose that the downcutting of the Verdon Gorges started approximately 1.5 to 2 Ma

---

\* Corresponding author.

ago, even if the drainage network of the Verdon catchment area could have been shaped earlier, during the Messinian salinity crisis.

**Keywords.** Quaternary, Geomorphology, CRE  $^{36}\text{Cl}$  dating, Fluvial incision, Gorges.

*Published online: 25 July 2023*

## 1. Introduction

Rivers, through their erosive power, play a key role in adjusting the landscapes to multiple forcings such as tectonic uplift, sea-level fluctuations or climate variations [Whipple, 2004, Whipple and Tucker, 1999]. Indeed, bedrock channels set the base level for adjacent hillslopes and thus control long-term relief evolution and denudation rates [e.g., Whipple *et al.*, 2000]. Rivers not only control mass wasting by undercutting hillslopes in mountainous areas [Howard *et al.*, 1994], they also transport the resulting sediments towards depositional basins in mountain forelands [Guerit *et al.*, 2016].

The rate at which river incision shapes landscapes is highly variable and is controlled by processes operating at different temporal and spatial scales [Daniels, 2008]. These processes interact with each other, and the study of short-term ( $<10^3$  yr) processes may allow to better understand their respective contributions together with longer-term forcings ( $>10^4$  to  $10^5$  yr). For example, as climate variations control water discharge in rivers [Ely, 1997], understanding how punctual flood events influence bedrock incision rates can provide insights on the long-term landscape sensitivity to climate changes [ $10^3$ – $10^4$  yrs, Molnar, 2007, Hartshorn *et al.*, 2002, Lague *et al.*, 2005]. Through the recurrence of short-term processes ( $<10^3$  yr), rivers are irrevocably adjusting their incision rates to long-term tectonic uplift rates in order to achieve an ideal steady state in which vertical incision equals to rock uplift [Whipple and Tucker, 1999, Wobus *et al.*, 2006]. However, deciphering the dominant forcing if any (e.g., tectonic vs. climate) remains difficult [Herman *et al.*, 2013].

The so-called “external” forcings control river erosion by providing the necessary tools for bedrock incision: water discharge and sediment availability. While the first provides the energy for sediment transport, the latter acts as a “mechanical tool” for rivers to incise their bedrock [Sklar and Dietrich, 2006, Jansen *et al.*, 2011]. However, several studies showed that an excessive amount of sediments will, to the contrary, prevent incision by overloading the

river, raising the channel bed by aggradation and therefore temporarily shielding the bedrock [Sklar and Dietrich, 2001, Hartshorn *et al.*, 2002]. Furthermore, the efficiency of bedrock incision is controlled by intrinsic morphological and geological features (lithology, slope, with/depth ratio, local relief [Schumm, 1977]. The degree of jointing and the weathering state of the bedrock also influence river incision rates [e.g., Whipple *et al.*, 2000]. These added elements together act as a “geological factor” that dictates the locus of erosion and its efficiency [Cowie *et al.*, 2008, Hartshorn *et al.*, 2002, Herman *et al.*, 2013, Sklar and Dietrich, 2001].

In fold-and-thrust belts, the folding of sedimentary layers with a distinct resistance to erosion produces complex river network geometries with alternating strike-parallel and perpendicular stream sections defining a transverse drainage pattern [Oberlander, 1965, Stokes *et al.*, 2008, Twidale, 2004]. Beside these local heterogeneities, large-scale regional horizontal tectonic movements can be detected in the shape of the river network by systematic changes in flow directions resulting from the planar deformation of the river network with its substrate [Guerit *et al.*, 2016]. On the other hand, vertical tectonic motions of the bedrock together with along-channel variations in the rock resistance to erosion will affect both the river longitudinal profile and the shape of surrounding hillslopes. The complete understanding of interactions between such small- and large-scale parameters and incision processes over large spatial and temporal scales is not yet achieved [Jansen *et al.*, 2011].

With the goal to shed some new light on the response of a river system to internal and external factors, we chose to study the High Verdon Gorges (HVG), located in the Southwestern Alps foreland (Figure 1A). The Verdon catchment presents the advantage of cross-cutting the whole Meso-Cenozoic sedimentary sequence of the southern subalpine fold-and-thrust belt, including highly resistant upper Jurassic limestones in which the HVG were carved. The Verdon River headwaters are located in an area

previously covered by Quaternary glaciers [Brisset *et al.*, 2015], while its outlet in the Durance river is near the junction between the Alpine deformation front and the Valensole foreland basin (Figure 1B). In this paper, we present new, and use some published [Cardinal *et al.*, 2022],  $^{36}\text{Cl}$  Cosmic Ray Exposure (CRE) datings of river-polished surfaces in the HVG and interpret them for the recent (Late Quaternary) period, and discuss a long-term (Pliocene to Quaternary) evolutionary scenario of the Verdon River in its Alpine and Mediterranean context.

## 2. Context

### 2.1. *Structural context and drainage patterns of the Verdon River*

The study area is located upstream of the foreland basin of the Southwestern European Alps (Figure 1A and B). The Castellane fold-and-thrust belt (also called the “Castellane Arc”) was first formed during the Pyrenean collisional phase (Cretaceous to Eocene) and underwent reactivation during the Oligocene due to the onset of Alpine collision and SW propagation of the Penninic front, which resulted in the development of an Oligocene foredeep filled with turbiditic sequences [Espurt *et al.*, 2012, Jourdon *et al.*, 2014]. During the Miocene, compressional deformation propagated outwards and caused the uplift of the sedimentary wedge together with the flexure and filling of the Valensole molassic basin in the foreland (Figure 1B). This deformation phase ended with the underthrusting of Neogene molassic sequences below the Digne Nappe during Late Miocene times [Schwartz *et al.*, 2017]. The Valensole basin is filled with marine to continental conglomeratic sequences, and erosional unconformities have been tentatively correlated to the Mio-Pliocene transition marked by the Messinian Salinity Crisis [Clauzon *et al.*, 1996, 2011, Hippolyte *et al.*, 2011]. The last marine sequences found in the Valensole basin are dated as Late Tortonian and correspond to shallow water molasses [Ford *et al.*, 1999, Ford and Lickorish, 2004]. Gravel deposits mark the end of sedimentation in the Valensole basin, the upper surface of which has been dated around 1.8 to 2 Ma; however, towards the Alpine front, alluvial cones continue to prograde on the basin, ending with the Balene breccia formation dated at 0.7 to 1 Ma [Dubar, 1984, Dubar *et al.*, 1998].

The arrival of coarse, detritic deposits in the Valensole basin in the early Quaternary (ca. 2.4 Ma) is interpreted as reflecting active tectonics on the Castellane Arc and/or cooler climatic conditions [Dubar, 1984, Dubar *et al.*, 1998].

With a length of 166.5 km and a catchment area of 2218 km<sup>2</sup>, the Verdon River is the main tributary of the Durance River. The Verdon River and its catchment have their headwaters in the Helminthoid flysch nappes (~2500 masl) and run towards the south through the unmetamorphosed Mesozoic sedimentary cover of the Alpine foreland. Near the city of Castellane, the Verdon course takes a turn upon encountering the outer folds and thrusts of the Castellane Arc and consequently flows in a W-E direction, wandering around and cutting across the fold axes [Chardonnet, 1943, Jorda, 1975]. From this point, the Verdon cuts its way through Jurassic limestones in which it dug one of the most impressive European gorges, the High Verdon Gorges (HVG, Figure 1A). Downstream, the Verdon River meets the Valensole Plateau and follows the Valensole conglomerate regular slope while repeatedly crossing some Jurassic limestone outcrops [Goguel, 1935], until it reaches its outlet in the Durance River (255 masl, Figure 1B). The longitudinal profile of the Verdon River reflects well lithological variations encountered along the channel length. Indeed, significant convexity can be seen where the river has incised the massive Tithonian limestone and formed the HVG, whereas upstream and downstream, the river profile, although modified by artificial dam lakes, is overall concave (Figures 1C and 2).

The origin of the Verdon River course is a matter of debate. Indeed, the upstream portion of the river trends roughly parallel to the N-S direction of tectonic structures [Goguel, 1935, Jorda, 1975]. Further its middle part crosscuts sub-perpendicularly the fold axes affecting the Jurassic cover, while encompassing the upper part of the HVG and the southern boundary of the Castellane Arc [Chardonnet, 1943], from the city of Castellane to the junction between the Verdon and Artuby rivers (Figure 1B). To explain these cross-cutting relationships, many authors agree on the hypothesis that the Verdon River course is, in the area, antecedent [Blanchard, 1915, Chardonnet, 1943, Goguel, 1935, Nicod, 2004]. This hypothesis implies that the Verdon River was originally flowing on a rather low-relief peneplane and

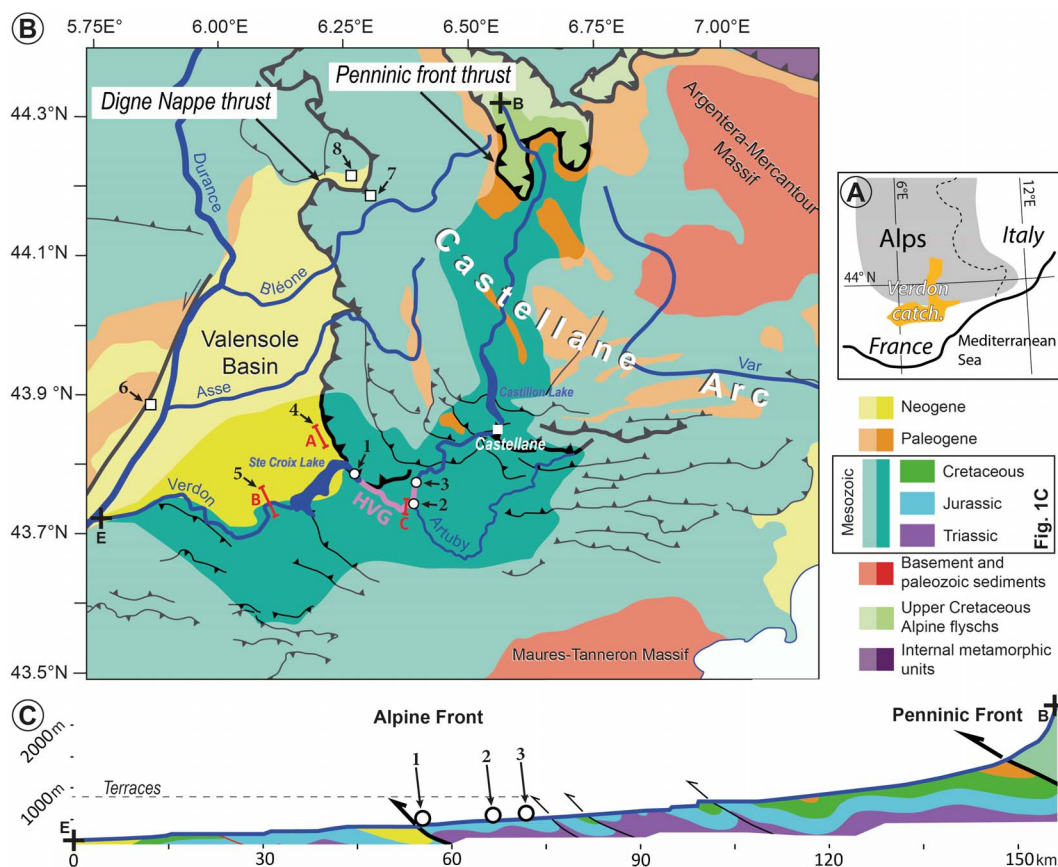


**Figure 1.** (A) Location of the Verdon Catchment in the Southwestern Alps. (B) Simplified geological map of the study area. The Verdon catchment area is underlined by brighter colours, corresponding to the colours in the legend and on the cross-section. The High Verdon Gorge (HVG) are highlighted along the river in pink. (C) Schematic geological cross-section along the Verdon River longitudinal profile. Black crosses indicate the beginning (B) and the end (E) of the river profile. Note that in the profile; Cretaceous, Jurassic and Triassic periods are distinguished from the more general term “Mesozoic” used in the geological map B, as highlighted in the legend. The Black outlined circles 1 to 3 on the map and on the profile indicate the sampling sites. Thick red lines A, B, and C show the location of the topographic profiles shown on Figure 10. Locations numbered 4 to 8 are incision or uplift rates from literature which are discussed in Section 5.

was then forced into incising the underlying Tithonian limestones during a Cenozoic tectonic uplift episode [Chardonnet, 1943].

## 2.2. Catchment morphology

The overall “L shape” of the Verdon catchment suggests possible drainage captures [Blanchard, 1915] and/or a complex adaptation to a deformed terrain [Goguel, 1935]. From a closer look, the Verdon

catchment and long river profile (Figure 1) can be divided into three portions:

- The upper Verdon Valley, from the headwaters to downstream of Castellane town;
- The HVG, knickzone interrupting the overall concave profile (Figure 2A);
- The lower Verdon Valley, from the Sainte Croix Lake to its junction with the Durance River.

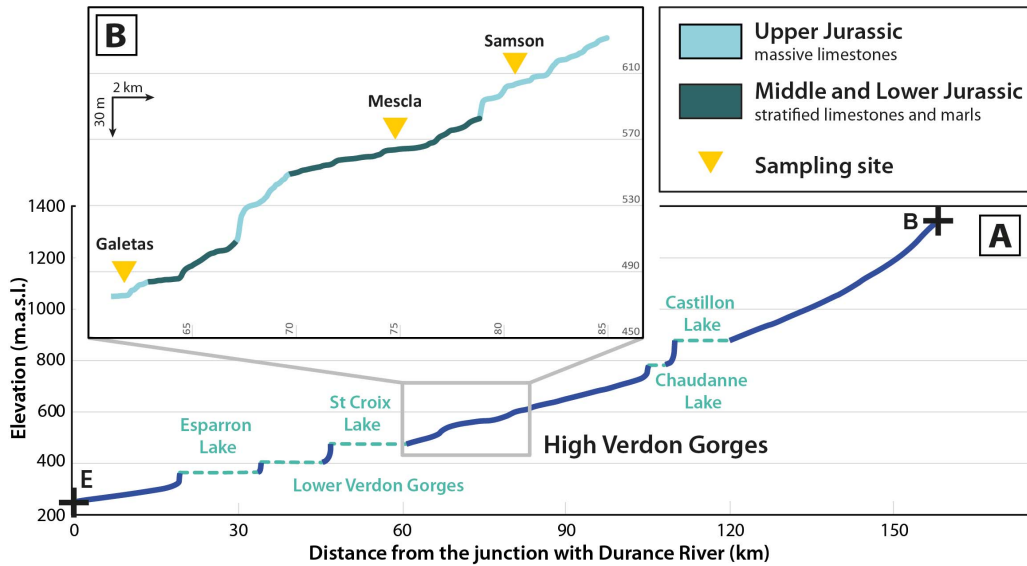


**Figure 2.** (A) Verdon River profile and location of the HVG and dam lakes. (B) Longitudinal profile of the Verdon River along the HVG, lithology schematic outcrop and location of the sampled sites. Black crosses indicate the beginning (B) and the end (E) of the river profile (see location of these point in Figure 1B).

Regarding the upper section, the Verdon River catchment width decreases downstream as a result of massive captures from the Asse and Bléone rivers to the West and from the Var River to the East [Blanchard, 1915, Chardonnet, 1943, Jorda, 1975]. These authors considered that the HVG constitutes an abnormally high local base level for the upper Verdon. The HVG forms a limestone (Tithonic) lithological knickpoint which likely mitigates the propagation of incision upstream, as observed in several studies [Crosby and Whipple, 2006, Jansen *et al.*, 2010, Bishop and Goldrick, 2010, Cardinal *et al.*, 2022]. Therefore, undergoing slower incision, the upper Verdon mean elevation remains high, which makes it vulnerable to capture by the more competitively erosive surrounding catchments. The high mean elevation also allowed extensive glacier coverage in the upper Verdon catchment. For comparison, the Würmian glaciers extent reached a length of 40 km along the Verdon River, against only 20 km along the Var River. The HVG therefore has a high impact on the morphological evolution of the upstream catchment. Between the Sainte Croix and Castillon lakes, the HVG course displays a complex pattern (Figure 1B). Downstream, the Verdon drainage area then considerably grows from the contribution of

the Artuby River (from 962 km<sup>2</sup> to 1300 km<sup>2</sup>) and the incorporation of the Valensole Plateau drainage network.

### 2.3. High Verdon Gorges morphology

The 26 km-long HVG (Figure 3A) appears as a deep cut in the massive limestones of the Mesozoic sequence. The cohesive nature of the bedrock results in maintaining steep walls with mean height around 300 m (Figure 3B, C), which makes it one of the most impressive mountain gorges in western Europe. However, the limestones show different facies along the gorges, from the compact late Jurassic to early Cretaceous Tithonian bars with limited jointing, to middle–upper Jurassic limestones and marls with a higher degree of bedding, fracturing and weathering (Figure 2). The lithological variations are visible on the river profile in the HVG, where Tithonian limestone outcrops are highlighted by strong knickpoints (Figure 2B). Furthermore, the gorge transversal profile is alternatively wide and narrow (Figure 3A), in agreement with the successive outcropping of middle–upper Jurassic and Tithonian limestones, respectively [Martel, 1908], demonstrating the contrast in rock resistance along the gorges.

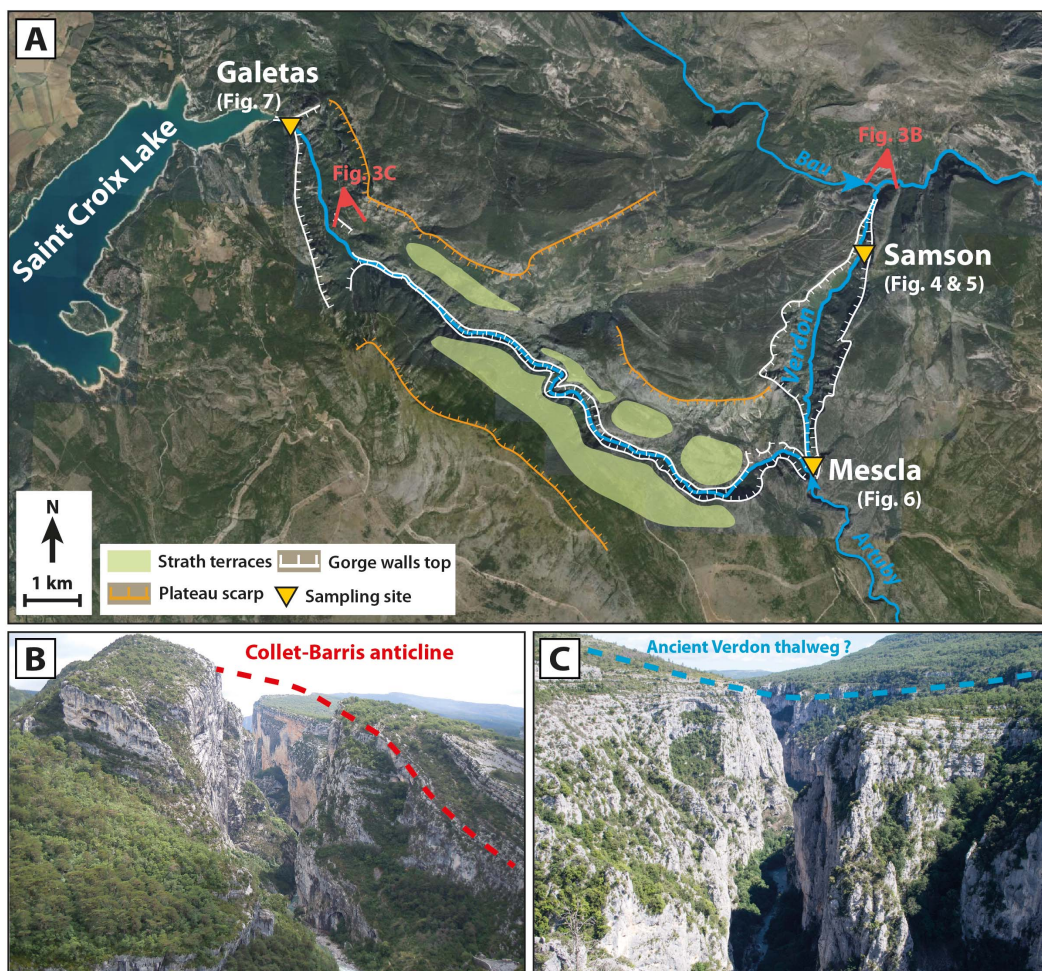


**Figure 3.** (A) Aerial image (IGN) of the HVG with the main topographic features and the location of the sampled sites and photos point of view (B and C). (B) Samson Corridor and location of the Collet-Barris anticline. (C) Location of the possible ancient Verdon thalweg position.

A combination of rock falls, fluvial and karstic erosive processes operates inside the gorges [Chardonnet, 1943, Martel, 1908, Nicod, 2004]. The gorge walls are affected by rock falls, creating scree slopes overgrown by vegetation at the foot of weak lithology walls and large boulder accumulations in the riverbed overlooked by resistant lithology walls. Intense fluvial erosion is visible through the widespread presence of pot-holes and polished surface, sometimes preserved high up in the steep walls but especially along the riverbanks and within the boulder accumulation in the river bed (Figure 4). Locally, the development of karst network results in open

cavities and large overhangs (called “baumes”; Figure 4). These cavities in turn guide the course of the river and focus the fluvial erosion. The karstic network is also intricately with the current riverbed. Indeed, a part of the river flow is incorporated into the subsurface karst system at “La Mescla” [Figure 3A, Blanchard, 1915, Fabre and Nicod, 1978].

#### 2.4. Incision of the High Verdon Gorges

The top of the HVG vertical walls are marked by a flat erosion surface (Figure 3A), possibly corresponding to a level of terraces as their slope does not match



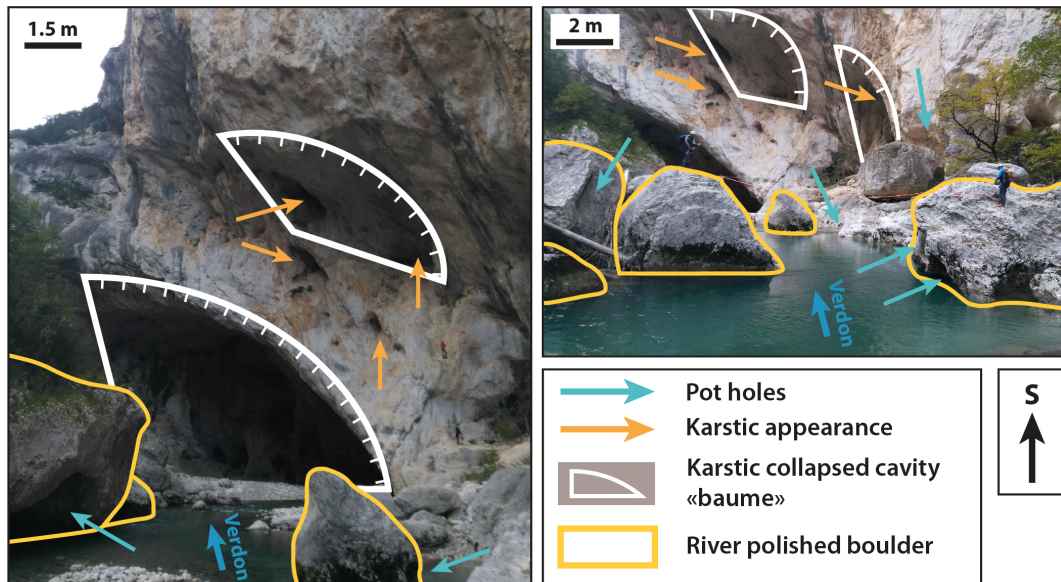


**Figure 4.** Field pictures of the High Verdon Gorges (at the vicinity of the Samson sampling site) and highlight of the main geomorphological erosion features.

that of the limestone bedding [Chardonnet, 1943]. Located between 800–850 masl, the terraces level is visible along the downstream part of the HVG, after La Mescla [Martel, 1908]. The terraces are not present in the upstream part of the HVG, but the numerous emergences of karstic network at the same altitude (800–850 masl) suggest that this paleo-level is continuous along the whole HVG [Chardonnet, 1943]. These terraces underline an ancient and wider river channel (Figure 3C), which is different from the present steep and narrow HVG.

No geochronological constraint is available to precisely determine the timing of incision and the formation of these terraces. However, some geological indices can help estimating the period at which the incision started. Indeed, continental deposits (conglomerates) from the Late Pleistocene, corresponding to the latest period of filling of the Valensole Basin, can be found at the same elevation as the terraces and karstic network, i.e., between 800–850 masl [Blanc, 1992, Chardonnet, 1943]. The event responsible for the onset of the HVG formation is believed to be the massive sea-level drop related to the Messinian Salinity Crisis [Blanc, 1992, Nicod, 2004], as proposed in surrounding areas [Clauzon *et al.*, 2011, Hippolyte *et al.*, 2011]. However, some authors

suggest that the formation of the HVG is not older than the Pliocene [Chardonnet, 1943]. From the elevation of the karstic network in the Lower Verdon Gorges (downstream of the St Croix Lake), Blanc [1992] estimated an incision rate of 0.34–0.33 mm/yr since the Pliocene-Quaternary boundary. However, no available data allows constraining incision rates for the recent Quaternary period.

### 3. Methods

#### 3.1. Sampling strategy

In order to bring new insights on the incision history of the HVG, three sites were selected and sampled for dating with the Cosmic Ray Exposure (CRE) method.

Considering the size of the HVG, it seemed more adequate to sample several sites along the gorges rather than one single wall as done previously in neighbouring areas [Valla *et al.*, 2010, Saillard *et al.*, 2014, Rolland *et al.*, 2017, Petit *et al.*, 2019, Cardinal *et al.*, 2021, 2022]. The main challenges in the HVG were the narrowness of the gorges and the along-strike lithological variations. Indeed, the portions of the gorges made of the most massive (Tithonian) limestones, in which well-preserved river polished

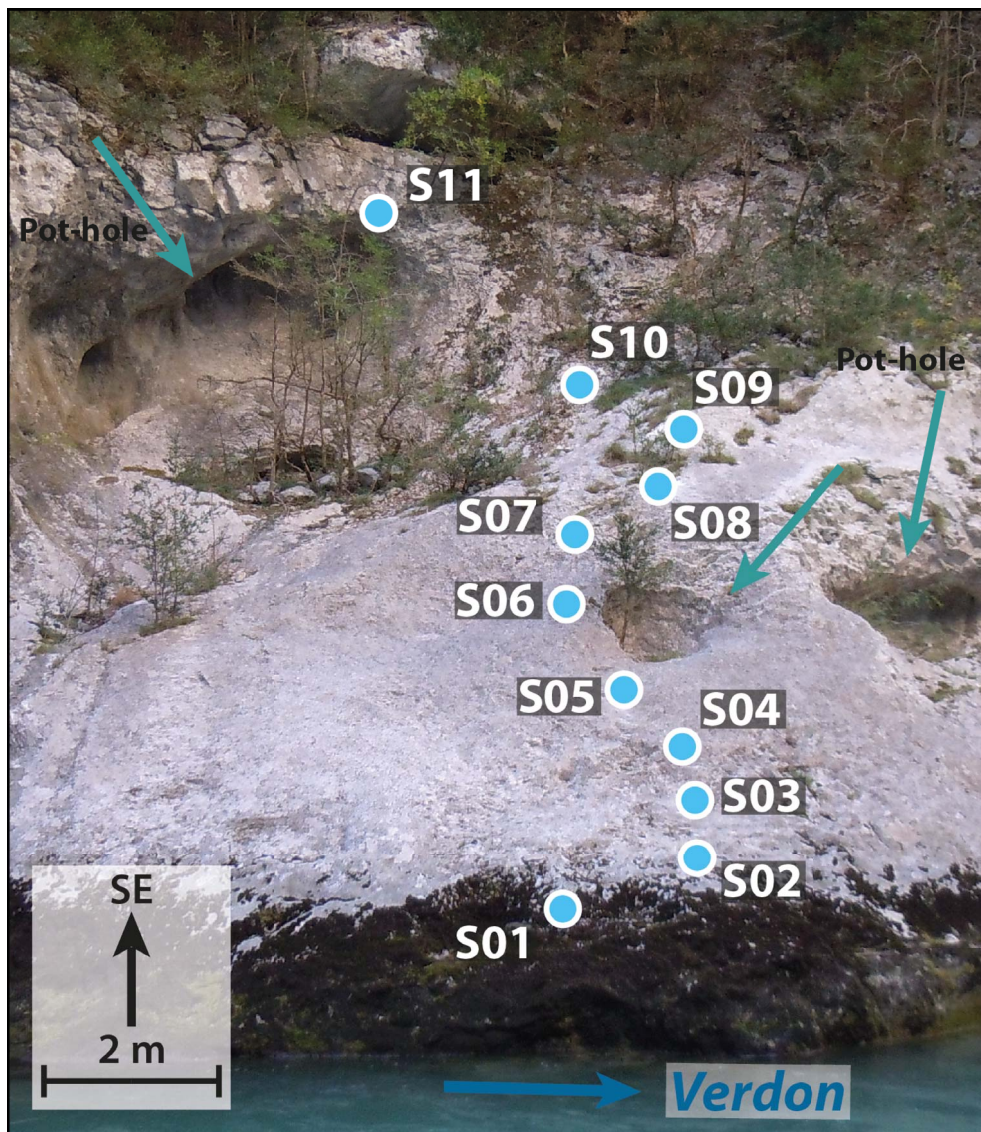


**Figure 5.** Field pictures of river-polished surface sampled in the Samson Corridor and sample locations. Note the presence of pot-holes attesting of the surface preservation since its exposure by incision.

surfaces can be expected, are also the narrowest ones, limiting exposure to cosmic rays due to strong topographic shielding. Conversely, well-exposed surfaces were found in portions of the gorges where the stratified limestones bedrock is very fractured and was most likely impacted by post-incision erosion process (mainly rock-falls). A compromise between gorge-wall preservation and reasonable topographic shielding resulted in the selection of three areas along the HVG (Figures 3, and 5–7) located in:

- The downstream part of the Samson Corridor, at the upstream entrance of the gorge;
- La Mescla, in the middle part of the gorges, at the junction with the Artuby River;
- The Galetas bridge, at the gorges outlet.

While being very narrow but well-preserved, the Samson Corridor opens up in its downstream part to a wide section of the gorge (Figure 3A),

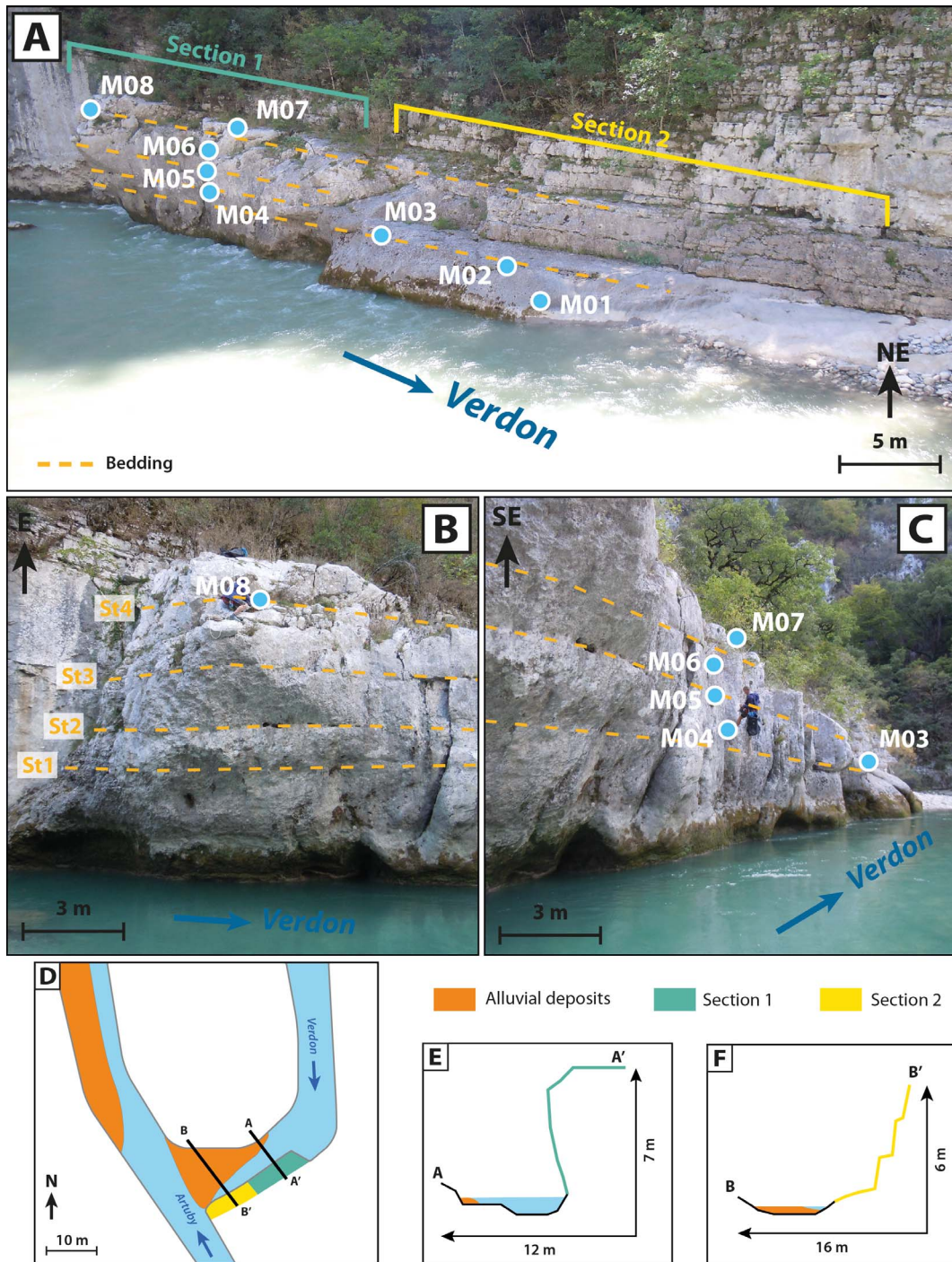


**Figure 6.** (A) Field pictures of river-polished surfaces sampled at La Mescla with sample location. Bedding (yellow dashed line) is gently dipping southwards ( $5^\circ$ ). (B, C) Details on Section 1 with overhanging walls. (D) Sketch map of the La Mescla site. (E, F) Schematic topographic cross-sections of Sections 1 and 2.

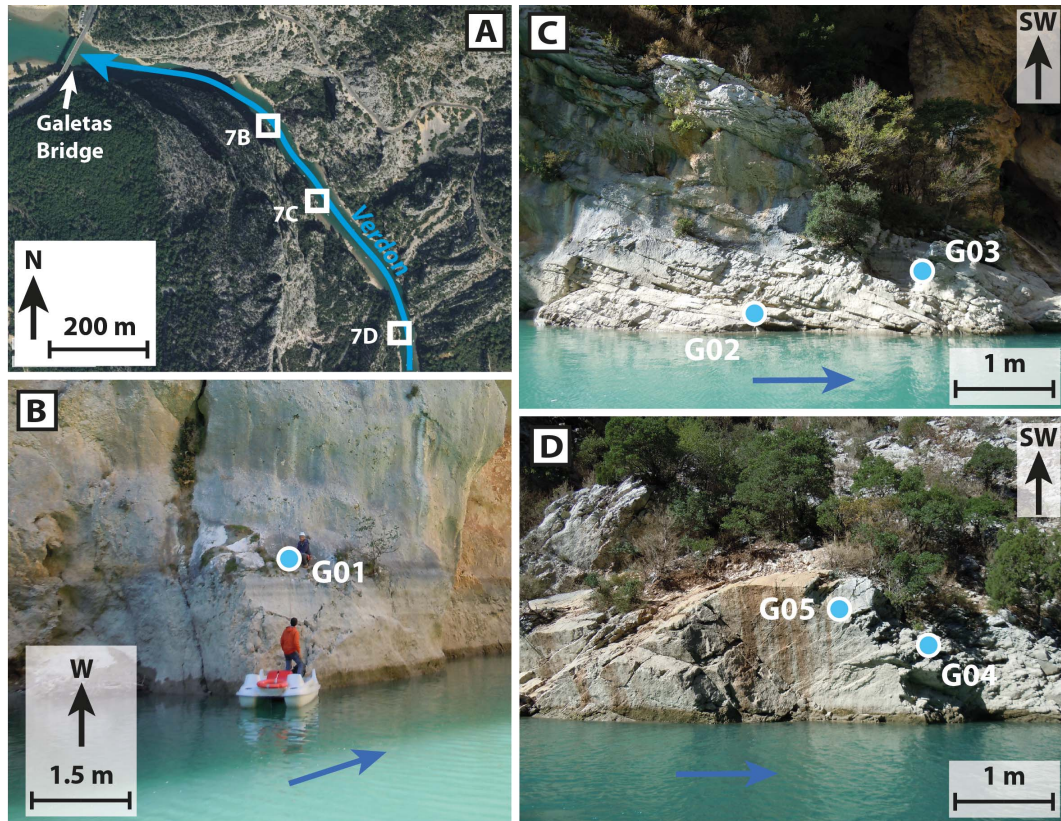


**Figure 7.** (A) Aerial image (IGN) of Galetas area and location of the three sampled river-polished surfaces. (B–D) Details of the three sampled river-polished surfaces and sample locations. Blue arrows show the river flow direction.

corresponding to a lithological change from massive to stratified limestone (Figure 2B). Sub-vertical polished surfaces showing good preservation with the presence of pot-holes were sampled (Figure 5).

La Mescla, is characterized by a deep meander at the junction with the Artuby River (Figure 3). Fluvial incision focused on the south flank by the tight curve of the meander has opened up this portion of the gorges and created a much wider space than in the direct surroundings, resulting in a more optimal exposure to cosmic rays. Although this portion of the gorges is characterized by thin and heavily fractured limestone beds, some river-polished features are visible in the thickest strata (Figure 6A–C). Two strikingly different polished surfaces were sampled (Figure 6). Section 1 (Green area, Figure 6A, D) is directly facing the entrance of the meander, while the second one is located slightly downstream, at the centre of the meander (yellow area, Figure 6A, D). The first section

shows an overhanging profile, with pot-holes in the lower part and underwater erosion pools at the foot of the wall (Figure 6B, C, E), while the second section shows a smoother, nearly flat profile in its lower part (Figure 6A, F). The site is also characterized by considerable sediment aggradation, creating a pebble cordon growing towards the Artuby River junction (Figure 6D).

At the Galetas bridge, we were confronted with the limit of accessibility, both from above, because of the height of the gorge walls, and below, because of the river depth. Therefore, instead of a vertical profile along a single wall, we choose to sample a longitudinal profile by sampling three polished surfaces at 8–10 m above the modern riverbed along the massive Tithonian beds that form the outlet of the HVG (Figure 7). The samples were collected with a hammer and chisel and their height above the river bed was measured with a tape measure.

### 3.2. $^{36}\text{Cl}$ CRE dating

$^{36}\text{Cl}$  concentrations in collected limestone samples were quantified in order to estimate Cosmic Ray Exposure (CRE) ages and unravel the exposure history of the steep (almost vertical) bedrock gorge walls that were theoretically gradually exposed through river incision [Schaller *et al.*, 2005, Ouimet *et al.*, 2008].  $^{36}\text{Cl}$  concentrations were determined by accelerator mass spectrometry (AMS) measurements performed at ASTER, the French national AMS facility (CEREGE, Aix-en-Provence) [Arnold *et al.*, 2010]. A sea-level and high-latitude  $^{36}\text{Cl}$  production rate for calcium spallation of  $42.2 \pm 3.4$  atoms  $^{36}\text{Cl} \text{ g}^{-1} \text{ a}^{-1}$  [Schimmelpfennig *et al.*, 2009, Braucher *et al.*, 2011] was used and scaled following Stone [2000] and corrected for topographic shielding (TS), constrained from field measurement data and using the online tool CRONUS-Earth from Balco *et al.* [2008]. For more details on the dating method and the analytical protocol, the reader is referred to several previous studies [Zerathe *et al.*, 2014, Cardinal *et al.*, 2021, 2022]. All exposure ages are indicated according to before present (BP) nomenclature.

### 3.3. Incision rate computation

The numerical code developed by Glotzbach *et al.* [2011], originally designed for thermochronology age-elevation relationships, was used to determine temporal variations in incision rates from the CRE data. The code defines the regression segments that best fit the CRE ages data and the associated uncertainties with elevation distribution. As in Glotzbach *et al.* [2011], a Monte Carlo approach was used to randomly divide the data into 1, 2 or 3 successive time intervals in order to define regression segments by weighted linear regression, and to select the best-fitting ones according to their  $R^2$  value. The following criteria were applied: no negative incision rate was allowed; regression segments constrained by less than 3 data points were rejected; the intersection between two curve segments must correspond to the intersection between the two sets of data that were used to calculate them.

## 4. Results and local interpretations

The sample characteristics are reported in Table 1. CRE ages determined from the  $^{36}\text{Cl}$  concentrations

are reported in the CRE age vs. height plots (Figure 8). The term “riverbed” used here refers to the bedrock, which corresponds to the bottom of the river channels. It was measured in few locations. The actual geometry of the river thalweg is therefore poorly constrained.

### 4.1. Samson Corridor

A total of 11 samples were collected along a 12 m-high polished surface in the Samson Corridor, which gave CRE ages ranging from 15 to 45 ka. These data were already presented by Cardinal *et al.* [2022], where the authors made a conservative choice to consider only one regression line for deriving incision rates. As in the present study, to constrain more precisely the timing of incision in the HVG, the code was allowed to use three regression lines in order to obtain incision rate variations. Apart from two samples (S10 and S11) that clearly demonstrate the occurrence of rock-falls [as seen in Cardinal *et al.*, 2021], the rest of the data shows a consistent history of progressive incision with three incision rate trends:

- $0.25 \pm 0.17$  mm/yr from 45 to 30 ka;
- $0.18 \pm 0.03$  mm/yr from 30 to 16 ka;
- $0.90 \pm 0.53$  mm/yr from 16 to 15 ka.

Considering the large uncertainties associated with the calculated incision rates, and relatively similar estimates, it can be concluded that the first two periods are difficult to distinguish from each other and that incision in the Samson Corridor underwent only one major incision rate change after ca. 16 ka. The lack of CRE data does not allow us to constrain an incision rate for the remaining 2 m of the surface, corresponding to the last 15 ka (Figure 8A).

### 4.2. La Mescla

Eight samples were collected along the two sections described above, and gave CRE ages ranging from 60 to 15 ka for Section 1 and 60 to 30 ka for Section 2. Both sections are located along the concave banks of the meander. The data collected from La Mescla indicate a much more contrasted incision history, which seems in agreement with the complex morphology of the site. Indeed, as described above, the sampled site can be seen as two distinct sections; an upstream part with an overhanging high wall, and a downstream part with a nearly flat surface. The top of each section

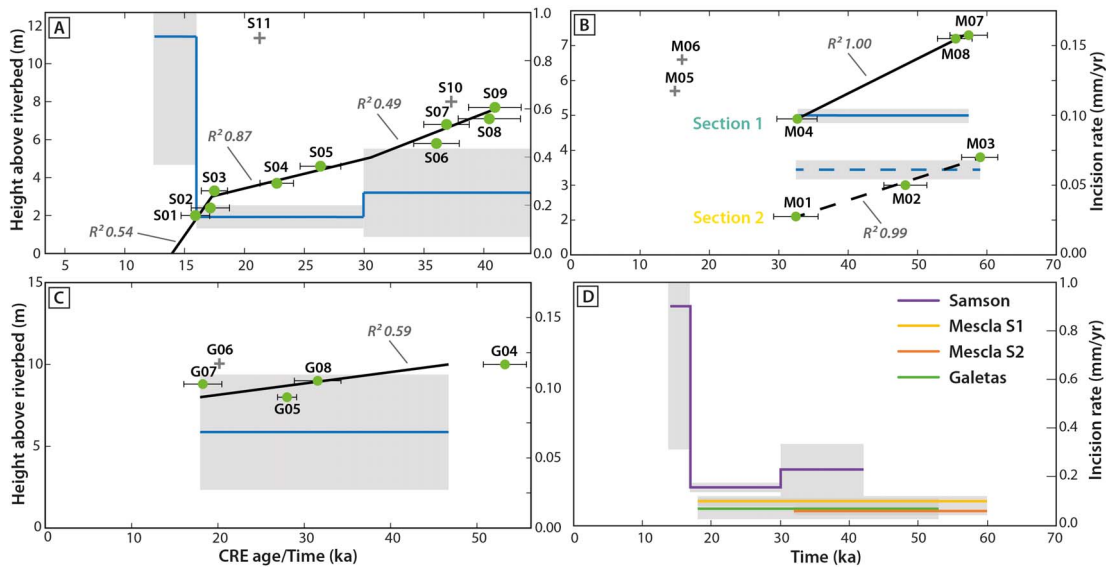


**Figure 8.** CRE age vs. height (left y-axis) plot and associated incision rates (right y-axis) of (A) Samson, (B) La Mescla with Section 1 (continuous line) and Section 2 (dashed line), and (C) Galetas. Black lines corresponds to linear regressions, blue lines corresponds to the incision rates inferred from those regressions and corresponding uncertainties (light grey rectangles). (D) Inferred incision rates variations over time for the studied sites, and corresponding uncertainties.

corresponds to the top of a limestone bed: St04 for the highest portion and St01 for the lowest portion (Figure 6A). Three observations can be made:

- Samples collected at the top of each of the two sections (03: Section 1; 07 and 08, Section 2) show similar exposure ages (55–60 ka), despite different heights above river bed (2.8 m for sample 03 and 6.2–6.3 m for samples 08 and 07);
- Samples 01 and 04, collected 2 m below the highest samples of their respective portion but at different heights above river bed (1.1 m for sample 01, 3.3 m for sample 04), have a similar exposure age (32 ka);
- Intermediate samples 05 and 06 (height above river bed: 4.7 m for sample 05 and 5.6 m for sample 06) both have a very similar age of 15–16 ka, much younger than the rest of the data, despite being located in an intermediate position relative to the river bed.

To understand these contrasted CRE ages, the evolution of this specific portion of the HVG must be reconstructed. The samples 08, 07 and 03, although lo-

cated at different heights above the present river bed, have similar exposure ages and could therefore represent a paleo-riverbed with a steeper slope than the present one (Figure 9A). The CRE age of samples 01 and 04 could then represent a second paleo-riverbed at ca. 30 ka, 2 m below the first one, but with a similar slope (Figure 9B). The CRE ages would therefore indicate that between 60 and 30 ka, incision occurred at a rate of 0.06–0.1 mm/yr.

However, Section 1 of La Mescla site seems to have undergone a more focused and intense incision, since the above mentioned tilted paleo-riverbed seems to have been flattened to match the modern riverbed. Indeed, Section 1 is directly facing the upper part of the meander, while Section 2 is located more deeply in the inside of the meander curve (Figure 6D). Hence, the upstream portion is more exposed to the direct impact of the river flow, while the downstream portion may be shielded from the shear strength and turbulence of the flow, as most of it is absorbed in the upstream section of the meander. Such a focused lateral erosion could have destabilized the bedrock wall by undercutting its foot, creating an overhanging cliff. Indeed, Samples 05 and 06

**Table 1.**  $^{36}\text{Cl}$  CRE sample characteristics and geochronological results

| Sample   | Height above river bed (m) | Samp. thick. (cm) | TS factor | Spallation scaling | $^{35}\text{Cl}$ (ppm) | Ca (%) | Atoms $^{36}\text{Cl}$ (at/g) | Atoms $^{36}\text{Cl} \pm$ (at/g) | CRE age (ka)   |
|--|----------------------------|-------------------|-----------|--------------------|------------------------|--------|-------------------------------|-----------------------------------|----------------|
| Samson (lat: 43.7842°; long: 6.3936°; mean elevation: 606 masl)    |                            |                   |           |                    |                        |        |                               |                                   |                |
| S01  | 2                          | 1                 | 0.16      | 1.67               | 37.3                   | 40.7   | 83,944                        | 6349                              | 15.9 $\pm$ 1.2 |
| S02  | 2.4                        | 1                 | 0.16      | 1.67               | 29.9                   | 40.7   | 89,670                        | 8452                              | 17.2 $\pm$ 1.6 |
| S03  | 3.3                        | 1                 | 0.16      | 1.67               | 32.5                   | 40.8   | 91,776                        | 5730                              | 17.5 $\pm$ 1.1 |
| S04  | 3.7                        | 1                 | 0.16      | 1.67               | 35.0                   | 40.7   | 118,596                       | 7068                              | 22.7 $\pm$ 1.4 |
| S05  | 4.6                        | 1                 | 0.16      | 1.67               | 31.5                   | 40.6   | 136,006                       | 8988                              | 26.4 $\pm$ 1.7 |
| S06  | 5.8                        | 2.5               | 0.16      | 1.67               | 32.0                   | 41.7   | 188,287                       | 9862                              | 36.0 $\pm$ 1.9 |
| S07  | 6.8                        | 1                 | 0.16      | 1.67               | 28.1                   | 40.8   | 187,869                       | 9775                              | 36.9 $\pm$ 1.9 |
| S08  | 7.1                        | 1                 | 0.16      | 1.67               | 28.6                   | 40.8   | 205,363                       | 13,024                            | 40.4 $\pm$ 2.6 |
| S09  | 7.7                        | 1.5               | 0.16      | 1.67               | 23.4                   | 40.7   | 205,909                       | 11,192                            | 40.9 $\pm$ 2.2 |
| S10*   | 8                          | 1.5               | 0.16      | 1.67               | 33.1                   | 40.6   | 190,457                       | 16,417                            | 37.3 $\pm$ 3.2 |
| S11*   | 11                         | 1                 | 0.16      | 1.67               | 24.5                   | 40.4   | 110,890                       | 8575                              | 21.6 $\pm$ 1.7 |
| La Mescla (lat: 43.7399°; long: 6.3794°; mean elevation: 564 masl) |                            |                   |           |                    |                        |        |                               |                                   |                |
| M01  | 1.1                        | 1                 | 0.39      | 1.61               | 43.1                   | 40.5   | 388,057                       | 38,470                            | 32.5 $\pm$ 3.2 |
| M02  | 2.0                        | 1                 | 0.39      | 1.61               | 47.3                   | 40.5   | 568,763                       | 36,811                            | 48.2 $\pm$ 3.1 |
| M03  | 2.8                        | 1                 | 0.39      | 1.61               | 33.5                   | 40.6   | 677,155                       | 29,949                            | 59.0 $\pm$ 2.6 |
| M04  | 3.9                        | 1                 | 0.39      | 1.61               | 36.5                   | 40.5   | 386,654                       | 34,273                            | 32.6 $\pm$ 2.9 |
| M05*   | 4.7                        | 3                 | 0.39      | 1.61               | 37.8                   | 41.1   | 184,681                       | 13,407                            | 15.0 $\pm$ 1.1 |
| M06*   | 5.6                        | 2.5               | 0.39      | 1.61               | 43.7                   | 41.1   | 198,667                       | 26,792                            | 16.1 $\pm$ 2.2 |
| M07  | 6.3                        | 2                 | 0.39      | 1.61               | 43.0                   | 40.7   | 669,682                       | 32,058                            | 57.4 $\pm$ 2.7 |
| M08  | 6.2                        | 1.5               | 0.39      | 1.61               | 49.3                   | 40.6   | 651,036                       | 29,465                            | 55.4 $\pm$ 2.5 |
| Galetas (lat: 43.7972°; long: 6.2576°; mean elevation: 475 masl)   |                            |                   |           |                    |                        |        |                               |                                   |                |
| G01  | 10                         | 1                 | 0.20      | 1.49               | 16.2                   | 40.5   | 288,596                       | 13,927                            | 53.2 $\pm$ 2.6 |
| G02  | 8.0                        | 1                 | 0.54      | 1.50               | 26.9                   | 40.5   | 423,770                       | 18,845                            | 28.0 $\pm$ 1.2 |
| G03*   | 10                         | 1                 | 0.54      | 1.50               | 19.5                   | 40.6   | 308,352                       | 15,745                            | 20.3 $\pm$ 1.0 |
| G04  | 8.9                        | 1                 | 0.67      | 1.49               | 48.6                   | 40.5   | 356,756                       | 18,990                            | 18.3 $\pm$ 1.0 |
| G05  | 9.0                        | 2.5               | 0.67      | 1.49               | 49.4                   | 41.1   | 596,356                       | 29,548                            | 31.6 $\pm$ 1.6 |

Sample field information, topographic shielding (TS) factor of the sampled surfaces, samples thickness (Samp. thick.), natural chlorine contents, calcium, cosmogenic  $^{36}\text{Cl}$  contents in the limestone samples, resulting  $^{36}\text{Cl}$  CRE ages are indicated. Samples with an asterisk correspond to CRE ages identified as outliers and discarded for incision rate computation.

show similar young exposure ages of  $\sim 16$  ka, which can be interpreted as rock falls. Indeed, although probably smoothed by dissolution, the shallow cavity scarred by a vertical fracture, in which samples 05 and 06 are located, could be indicative of a rock fall (Figure 6C) and therefore could explain the much younger CRE age of those samples compared to the surrounding ones. The CRE data agree with an acceleration of incision at the same time for the Samson

area (Figure 8A), suggesting a period of enhanced incision occurring around 16 ka (age of the possible rock falls). Such an incision wave could have flattened, very locally and by a combination of vertical incision and lateral erosion, the riverbed by erasing what could have been a small lithological knickpoint at La Mescla that did not propagate upstream, as observed in other studies [Johnson et al., 2010, and references therein].

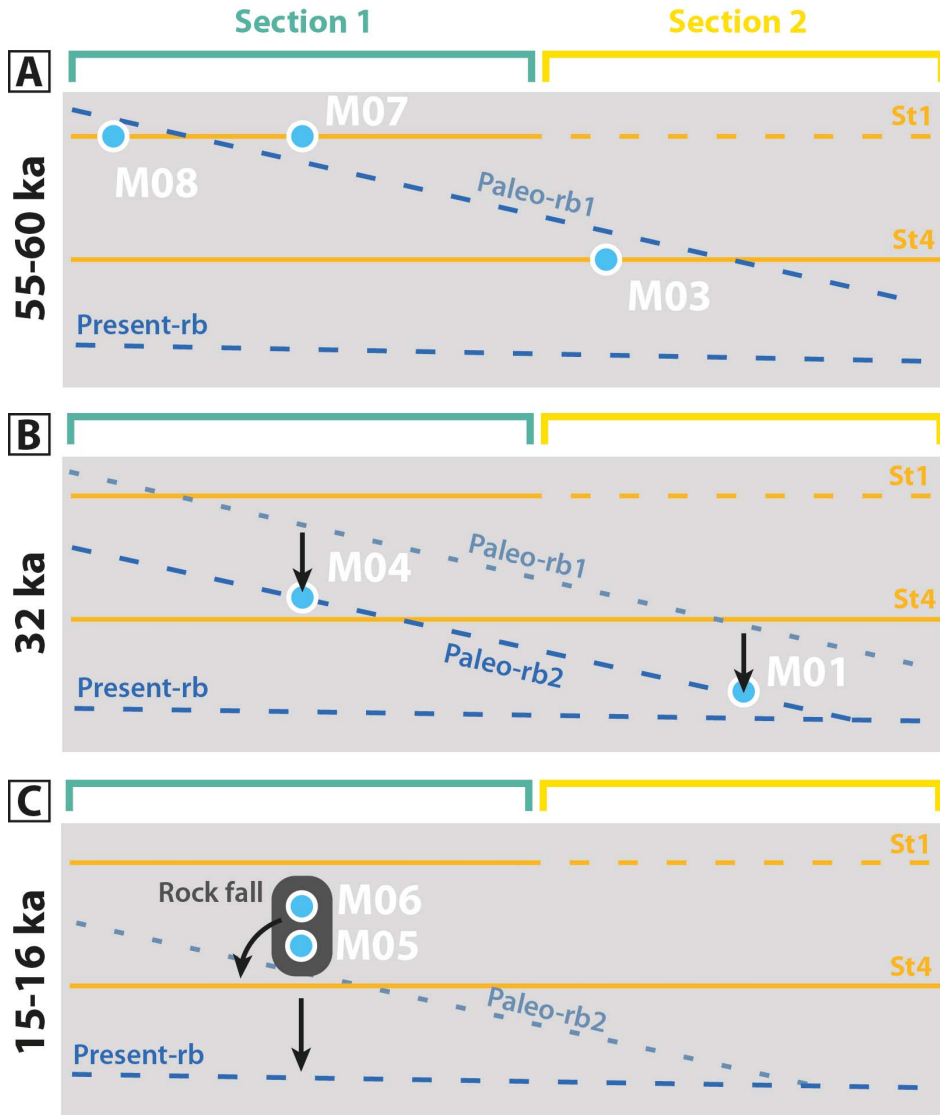


**Figure 9.** Sketch (not to scale) of the proposed evolution and incision history of the La Mescla sampled site at (A) 55–60 ka, (B) 32 ka and (C) 15–16 ka. Paleo-rb: proposed slope of paleo-riverbed; Present-rb: estimated present riverbed slope; St: limestone strata. The term “riverbed” used here refers to the bedrock, which corresponds to the channel bottom.

#### 4.3. Galetas

A total of 5 samples was collected along three river polished surfaces at the outlet of the HVG. The CRE ages range between 55 and 15 ka. The compilation of these data suggest a low and yet poorly constrained incision rate of  $0.07 \pm 0.04$  mm/yr between the 15–55 ka period.

## 5. Discussion

### 5.1. Short-term incision

The code was allowed to calculate incision rates with relatively few points, permitting to highlight rapid variations in incision rates. The disadvantage of this approach is that these incision rates are not always



well constrained from the CRE data. This strategy allows us to infer an acceleration of incision from 0.2 to 0.9 mm/yr between 17 and 15 ka in the Samson Corridor (Figure 8C), but with too few points to really constrain it. At the same period, a sequence of rock falls in the La Mescla site can be inferred, suggesting a period of increased downcutting at that time. Following the regional interpretation proposed by Cardinal *et al.* [2022], several rivers connected to the Last Glacial Maximum (LGM) glaciation in the SW French Alps underwent a period of enhanced fluvial incision following the main glacier retreats [19–17 and 14 ka; Rolland *et al.*, 2019]. From these results, it seems that the Verdon River may have undergone the same evolution, but since only three ages younger than 20 ka are obtained in the entire dataset, it remains difficult to infer any detailed post-glacial history of the HVG with confidence.

## 5.2. Long-term incision

Our results yield two ranges of slow but steady incision rates for the HVG: 0.06–0.07 mm/yr in the downstream parts of the HVG (Galetas and La Mescla Section 2), a roughly similar value of 0.1 mm/yr in the area of focused incision (La Mescla Section 1) between 60 and 15 ka (Figure 8C), and a larger value around 0.2 mm/yr on average in the upstream part (Samson Corridor) of the HVG.

Based on these estimates and on data obtained on the HVG by CRE dating, the following questions can be subsequently explored: (1) What is the onset time of HVG formation? (2) What is the main driver for the long-term incision? (3) What is the respective contribution of glacial/interglacial phases in lowering or enhancing these long-term incision rates?

### 5.2.1. What is the onset time of HVG formation?

From the CRE data, the long-term Verdon River incision rates can be bracketed between 0.06 and 0.2 mm/yr on scales up to several 10's of ka (neglecting the brief, less constrained, 0.9 mm/yr incision rate ~at 15 ka obtained in the Samson Corridor). These incision rates are lower than those inferred by Brocard *et al.* [2003] in the neighboring Buech river (0.8 mm/yr over the last 190 ka). If these results are extrapolated from the bottom of the gorge to the first level of terraces, up to 300 m above the present riverbed near La Mescla (Figure 10), computed

first-order ages estimates range between 1.5 and 5 Ma, which would thus represent the onset of the main incision period that dug the HVG up to 300 m.

The last deposits of the Valensole basin are dated around 1.8 to 2 Ma [Dubar, 1984, Dubar *et al.*, 1998, Hippolyte *et al.*, 2011], except for local clastic deposits of the Balene breccia formation, which are dated around 0.7 to 1 Ma [Dubar *et al.*, 1978, 1998]. This continental formation is presently incised by tributaries of the Verdon River. The upstream position of this formation suggests that downcutting of the lower Verdon River may have started before 1 Ma [Dubar *et al.*, 1998]. In that case, the maximum height of the HVG (~300 m) would correspond to a long-term incision rate of 0.3 mm/yr, which is higher but of the same order of magnitude than short-term rates deduced from CRE data.

The end of sediment deposition in the Valensole basin is ascribed to Early Quaternary climate cooling, and was supposed to correspond to the onset of river network entrenchment in the Valensole plateau and its surroundings [Dubar, 1984]. While global cooling started in the late Pliocene for the Northern hemisphere [Suc and Zagwijn, 1983, Haug *et al.*, 2005], evidence for increased incision and valley downcutting in the Alps seem to have occurred later, around 0.9–1 Ma [Muttoni *et al.*, 2003, Valla *et al.*, 2011], hence around the mid-Pleistocene transition between the glacial/interglacial cycles periodicity of 40-ka to 100-ka [Lisiecki, 2010]. Therefore, the onset of the Valensole basin deposits incision can be bracketed between 1 and 2 Ma, which is consistent with the younger age estimate (ca. 1.5 Ma) of gorge entrenchment and the higher bound of incision rates (~0.2 mm/yr) estimated from our CRE datings and extrapolation along the HVG.

### 5.2.2. What is the main driver for the long-term incision?

The present total incision of the Balene breccia formation, located in the Valensole Basin, is of 50 to 70 m, leading to a mean incision rate of 0.07 to 0.1 mm/yr over the last 0.7–1 Ma. Between the Valensole abandonment surface dated at 1.8 to 2 Ma and the Verdon thalweg around the Sainte Croix Lake, it can be estimated that the Verdon River has incised about 220 m, which gives a mean incision rate of 0.1 mm/yr since that time. This estimate is consistent with the above mentioned estimation obtained

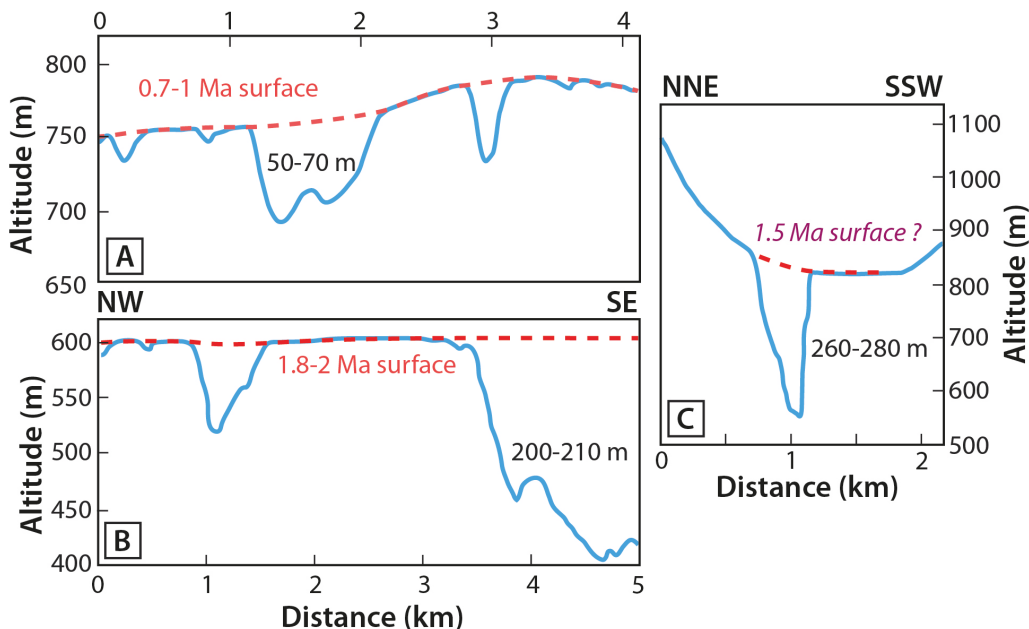


**Figure 10.** Topographic profiles drawn from the IGN DEM with corresponding surface abandonment ages. (A) across the Valensole Plateau near Moustier Sainte Marie; after Dubar *et al.* [1998], (B) along the lower Verdon channel; after Dubar *et al.* [1998] and (C) in the HVG near the La Mescla site (this study). See location profiles on Figure 1B. Note that the vertical and horizontal scales are different between each panel.

from the Balene breccia formation (Table 2). From morphological analysis and CRE dating of the Durance terraces, Siame *et al.* [2004] inferred a similar incision rate for the Durance River on its eastern side, with rates of 0.1 mm/yr since 2 Ma. The value of 0.1 mm/yr can therefore be assumed to constitute a good estimate for the long-term (i.e., since 1.8 to 2 Ma) average incision rate of rivers in the Valensole plateau. Such an incision rate is possibly driven by large-scale isostatic and/or tectonic uplift [Champagnac *et al.*, 2008], although local tectonic structures might have also played a role [Hippolyte and Dumont, 2000, Siame *et al.*, 2004].

This mean incision rate of 0.1 mm/yr is roughly consistent with the higher range of incision rates inferred for the medium part of the HVG: “La Mescla” site and, considering its large uncertainties, and the Galetas site in the lower part of the HVG. It is also consistent with contemporary average denudation rates ranging between 0.04 and 0.12 mm/yr computed from topographic analysis and  $^{10}\text{Be}$  CRE data on the Valensole Plateau hillslopes [Godard *et al.*, 2020]. Incision rates in the Samson Corridor

(0.2 mm/yr) is twice as high, as in neighbouring catchments for the recent period covering the last ca. 40 ka [ranging from 0.15 and 0.28 mm/yr; Cardinal *et al.*, 2022]. This can be ascribed either to differential tectonic motions (with respect to the lower Verdon Gorges and Valensole plateau) or to delayed incision of a steep, disequilibrium river profile that might have accumulated between several glacial cycles [Rolland *et al.*, 2017]. The tectonic hypothesis argues for the role of Pliocene to Quaternary faults, accommodating Plio-Quaternary shortening along the Digne–Castellane arcs [e.g., Sanchez *et al.*, 2010, Bauve *et al.*, 2014]. These structures could locally consist of EW trending blind thrusts and folds responsible for the measured incision rates in the Samson Corridor. For instance, in the Samson Corridor, the Verdon River cuts across a topographic dome corresponding to an anticline axis cored by lower Jurassic limestones (the Collet-Barris anticline), instead of flowing in the neighbouring, lower-altitude syncline to the west (Figures 1C and 3B). This can be interpreted as an antecedence assisted by the network of N–S and E–W faults [Nicod, 2004] and suggests

**Table 2.** Synthesis of incision and uplift measurements estimates in the study area

| Time interval (ka) | Uncertainty (ka) | Height (m) | Uncertainty (m) | Observation | Site name         | Site number       | Reference                            |
|--------------------|------------------|------------|-----------------|-------------|-------------------|-------------------|--------------------------------------|
| 20                 | 1                | 1.4        | 0.5             | Incision    | Galetas           | 1                 | This study                           |
| 30                 | 5                | 2          | 0.5             | Incision    | Mescla            | 2                 | This study                           |
| 50                 | 5                | 10         | 0.5             | Incision    | Samson            | 3                 | This study                           |
| 850                | 150              | 60         | 10              | Incision    | Balene breccia    | 4                 | [Dubar, 1984] and this study         |
| 1900               | 100              | 200        | 10              | Incision    | Valensole surface | 5                 | [Dubar et al., 1998] and this study  |
| 2000               | 100              | 200        | 50              | Uplift      | East Durance      | 6                 | [Siame et al., 2004]                 |
| 1450               | 100              | 290        | 10              | Incision    | Samson            | 3 <sub>ext</sub>  | This study (extrapolated)            |
| 3000               | 400              | 345        | 5               | Uplift      | Digne nappe       | 7                 | [Hippolyte et al., 2011]             |
| 3000               | 400              | 645        | 5               | Uplift      | Digne nappe       | 7 <sub>corr</sub> | [Hippolyte et al., 2011] (corrected) |
| 6000               | 500              | 3500       | 500             | Denudation  | Velodrome         | 8                 | [Schwartz et al., 2017]              |

Site numbers and location refer to Figure 11.

a possible, very slow differential uplift between the Mesozoic sedimentary cover units of the Castellane arc and the Valensole basin of 0.1 mm/yr since the incision onset of the HVG. This value is consistent with previously obtained estimates of differential uplift rates on Quaternary canyons in the Digne Nappe, although the age of the canyons are only indirectly constrained [Hippolyte et al., 2011]. The contractional deformation is still ongoing, as shown by the seismicity observed south of the Castellane area [see Le Pichon et al., 2010, Larroque et al., 2021 for a synthesis].

To the Northwest of the HVG, thermochronology data from Miocene sediments underthrust below the Digne Nappe yielded long-term exhumation rates of about 0.5 to 0.6 mm/yr since ca. 6 Ma [Figure 11C; Schwartz et al., 2017]. These higher values are possibly due to the activity of a crustal-scale, “thick-skin”, thrust located below the Barles half-window [Nouibat et al., 2022, Schwartz et al., 2017]. Here, NNW–SSE to NW–SE trending thrust wedges (Esclançon and Tanaron horse structures) have accommodated N70°E-trending compressional deformation and are responsible for the Plio-Quaternary uplift of Barles area [Hippolyte et al., 2011]. In addition, based on balanced and restored cross-sections through southwestern Subalpine and Central Provençal zones, Balansa et al. [2022] suggested that the relative northeastward migration of

buried basement highs contributed to the observed Pliocene-Quaternary contractional deformation and uplift of the central and northern extremity of the Valensole area. It is likely that this contractional deformation continued to migrate to the NNE until reaching the Barles half-window. The above mentioned local exhumation rates are consistent with the preservation of late Pliocene to early Quaternary canyons in the Digne Nappe, as denudation can have been more focused and more intense in the Barles half-window than in the surrounding area, where the nappe is preserved and well visible today. Moreover, the late stage denudation history since 1–2 Ma is too recent and too shallow to be precisely recorded by apatite fission-track (AFT) and (U–Th)/He (AHe) thermochronology data.

Considering all these values together, and assuming that recent (<60 ka) incision rates in the HVG can be extrapolated to the overall Quaternary period, it can be proposed that: (i) there is a very slow (0.1 mm/yr) uplift of the whole region since the last 1.5 to 2 Ma, encompassing the Valensole basin and the Digne Nappe–Castellane Arc units, which is possibly the result of late Alpine tectonics or isostatic uplift [e.g. Champagnac et al., 2008]; (ii) there might be an additional, although very slow, thin-skin deformation (0.1 mm/yr of uplift) of the sedimentary cover of the Castellane Arc relative to the Valensole basin; (iii) the situation is different in the

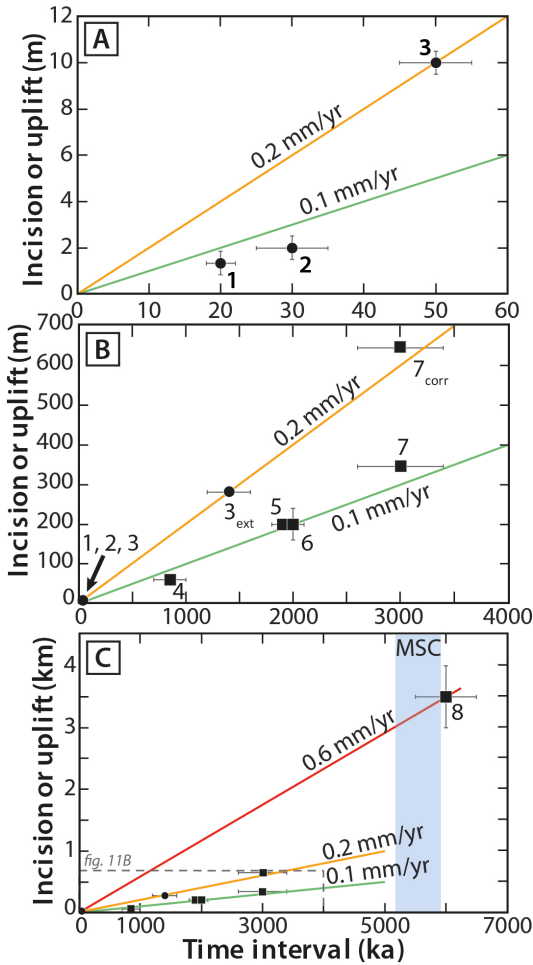


**Figure 11.** Compilation of incision and uplift rates at different time scales. (A) Incision rates in the HVG from CRE dating (this study) over 20 to 50 ka. (B) Same data as on A with additional incision or uplift rate estimates from the literature (sites 4, 5, 6 and 7). Point 3<sub>ext</sub> corresponds to the extrapolation of the recent 0.2 mm/yr incision rate (site 3) to the actual gorge height measured in the Verdon canyon. Points 7<sub>corr</sub> corresponds to the uplift of the Digne Nappe in the Esquichiere canyon relative to the Valensole basin [Hippolyte *et al.*, 2011, point 7], to which is added an uplift of 0.1 mm/yr of the Valensole basin relative to the base level, in order to allow comparison with the other points. (C) Same as B (B corresponds to the grey-dashed rectangle on the bottom left) with long-term AFT/AHe exhumation rate estimates from Schwartz *et al.* [2017] interpreted as uplift estimates. The Messinian Salinity Crisis (MSC) period is indicated (transparent blue rectangle). See Table 1 for details.

Barles half-window, where higher rock exhumation rates occurred in the Late Miocene (ca. 6 Ma) in response to the activity of a crustal-scale thrust [recognized on crustal-scale geophysical images; Nouibat *et al.*, 2022] and/or northeastward migration of a basement high [Schwartz *et al.*, 2017, Balansa *et al.*, 2022, Nouibat *et al.*, 2022]. Whether this activity was constant during the last 6 Ma, or was initially very fast and progressively slowed down to reach the observed uplift/incision rates for the last 1.5–2 Ma further south is difficult to quantitatively assess. Vertical GPS motions in the study area are poorly constrained, with present-day uplift rates of  $0.41 \pm 0.58$  mm/yr at the nearest station at Moustier-Saint-Marie [Sternai *et al.*, 2019], so it is impossible to compare our long-term uplift estimates values with modern and almost instantaneous uplift rates from geodesy [e.g., Piña Valdés *et al.*, 2022].

### 5.3. What is the respective contribution of glacial/interglacial phases in lowering or enhancing incision?

In this framework, and comparing our results with long-term incision rates estimated in the Valensole Plateau and in the Verdon Gorges, the higher (up to 0.9 mm/yr at 15–16 ka, Figure 8A) incision rates obtained in the Samson Corridor can be tentatively ascribed to its upstream position in the HVG. The Samson Corridor is located at the boundary between two erosion regimes during the late-Quaternary period. Incision is mainly controlled by the influence of glaciation in the high Verdon Valley, while the lower Verdon Valley is only under a fluvial incision regime. Therefore, the higher incision rates estimated over a short period ( $\sim 0.9$  mm/yr from 16 to 14 ka) could be the result of a paraglacial crisis in the Verdon River posterior to the LGM. The same timing of enhanced incision is observed in neighbouring catchments following post-LGM deglaciation [Cardinal *et al.*, 2022]. Furthermore, increased incision after 16 ka could have triggered rock falls in the La Mescla site of the HVG (Section 4.2). However, it is also possible that rockfall might solely be related to freezing and thawing effects, as observed by Cardinal *et al.* [2021] in a similar periglacial gorge setting. Therefore, the enhanced incision in the higher part of HVG could result from an increased interaction with the High Verdon Valley, where glacial incision has been efficient.

The effect of enhanced incision following glaciers melting could have been hindered and buffered in the rest of the gorges, due to the resistance of the Tithonian limestones to such influences.

## 6. Conclusions

We sampled three 10 m-high river-polished walls within the High Verdon Gorge, in order to apply the Cosmic Ray Exposure dating approach and derive incision rates. These data are used to discuss the gorge origin and both short-term and long-term dynamics. Each site shows local complexities related to the intricate course of the Verdon River and, except for the upstream boundary of the HVG (Samson corridor), no significant variations in incision rates with time are evidenced. It remains therefore difficult to relate the HVG downcutting to the post-LGM paraglacial incision crisis, as it is more likely the case in other rivers also connected to the LGM glacial extent in the region [e.g. Cardinal *et al.*, 2022]. The relatively steady incision rates (0.06–0.2 mm/yr) obtained from our CRE data cover a time window between 60 and 15 ka and are comparable to long-term regional uplift, exhumation and denudation rate estimates. This leads us to propose that tectonic and/or isostatic uplift are the main drivers for the Late Quaternary incision of the Verdon River. Finally, this long-term incision, when extrapolated to the rest of the vertical 300 m-high gorge walls and to other estimated incision heights from the Valensole basin, is consistent with a Mid- to Early Quaternary (~1.5 to 2 Ma) onset of incision for the HVG. This age estimate could reasonably fit with the beginning of Alpine glaciations; although the general pattern of the river network was probably already present in Late Miocene times, intense downcutting responsible for the initial entrenchment of the Verdon River can be ascribed to the Quaternary climate cooling.

## Conflicts of interest

Authors have no conflict of interest to declare.

## Acknowledgments

This study has been funded by the French Geological Survey (Bureau de Recherches Géologiques

et Minières; BRGM) through the national program “Référentiel Géologique de France” (RGF-Alpes). This work has also been supported by the French Government, through the UCA-JEDI Investments in the Future project managed by the National Research Agency (ANR) with the reference number ANR-15-IDEX-01. The  $^{36}\text{Cl}$  measurements were performed at the ASTER AMS national facility (CEREGE, Aix en Provence) which is supported by the INSU/CNRS, the ANR through the “Projets thématiques d’excellence” program for the “Equipements d’excellence” ASTER-CEREGE action and IRD. This manuscript benefitted from constructive reviews by two anonymous reviewers and efficient editorial handling by O. Fabbri.

## References

- Arnold, M., Merchel, S., Bourlès, D. L., Braucher, R., Benedetti, L., Finkel, R. C., Aumaître, G., Gottang, A., and Klein, M. (2010). The French accelerator mass spectrometry facility ASTER: improved performance and developments. *Nucl. Instrum. Methods Phys. Res. B*, 268, 1954–1959.
- Balansa, J., Espurt, N., Hippolyte, J.-C., Philip, J., and Caritg, S. (2022). Structural evolution of the surimposed Provençal and Subalpine fold-thrust belts (SE France). *Earth Sci. Rev.*, 227, article no. 103972.
- Balco, G., Stone, J. O., Lifton, N. A., and Dunai, T. J. (2008). A complete and easily accessible means of calculating surface exposure ages or erosion rates from  $^{10}\text{Be}$  and  $^{26}\text{Al}$  measurements. *Quat. Geochronol.*, 3, 174–195.
- Bauve, V., Plateaux, R., Rolland, Y., Sanchez, G., Bethoux, N., Delouis, B., and Darnault, R. (2014). Long-lasting transcurrent tectonics in SW Alps evidenced by Neogene to present-day stress fields. *Tectonophysics*, 621, 85–100.
- Bishop, P. and Goldrick, G. (2010). Lithology and the evolution of bedrock rivers in post-orogenic settings: Constraints from the high elevation passive continental margin of SE Australia. In *Australian Landscapes*, Geological Society, London, Special Publications, 346, pages 267–287. Geological Society of London.
- Blanc, J.-J. (1992). Signification géodynamique des réseaux karstiques étagés du canyon de Baudinard (moyennes gorges du Verdon). *Karstologia*, 20(1), 37–48.

- Blanchard, R. (1915). L'hydrographie du bassin supérieur du Verdon. *Rev. Géogr. Alp.*, 3(1), 57–67.
- Braucher, R., Merchel, S., Borgomano, J., and Bourlès, D. L. (2011). Production of cosmogenic radionuclides at great depth: a multi element approach. *Earth Planet. Sci. Lett.*, 309, 1–9.
- Brisset, E., Guiter, F., Miramont, C., Revel, M., Anthony, E. J., Delhon, C., et al. (2015). Lateglacial/Holocene environmental changes in the Mediterranean Alps inferred from lacustrine sediments. *Quat. Sci. Rev.*, 110, 49–71.
- Brocard, G. Y., van der Beek, P. A., Bourlès, D. L., Siame, L. L., and Mugnier, J.-L. (2003). Long-term fluvial incision rates and postglacial river relaxation time in the French Western Alps from <sup>10</sup>Be dating of alluvial terraces with assessment of inheritance, soil development and wind ablation effects. *Earth Planet. Sci. Lett.*, 209, 197–214.
- Cardinal, T., Audin, L., Rolland, Y., Schwartz, S., Petit, C., Zerathe, S., and Aster Team (2021). Interplay of fluvial incision and rockfalls in shaping periglacial mountain gorges. *Geomorphology*, 381, article no. 107665.
- Cardinal, T., Petit, C., Rolland, Y., Audin, L., Schwartz, S., Valla, P. G., et al. (2022). Fluvial bedrock gorges as markers for Late-Quaternary tectonic and climatic forcing in the Southwestern Alps. *Geomorphology*, 418, article no. 108476.
- Champagnac, J.-D., van der Beek, P., Diraison, G., and Dauphin, S. (2008). Flexural isostatic response of the Alps to increased Quaternary erosion recorded by foreland basin remnants, SE France. *Terra Nova*, 20(3), 213–220.
- Chardonnet, J. (1943). Le relief du Grand Cañon du Verdon. *Bull. Assoc. Géogr. Fr.*, 20(157), 87–97.
- Clauzon, G., Fleury, T.-J., Bellier, O., Molliex, S., Mocochain, L., and Aguilar, J.-P. (2011). Morphostructural evolution of the Luberon since the Miocene (SE France). *Bull. Soc. Géol. Fr.*, 182(2), 95–110.
- Clauzon, G., Suc, J.-P., Gautier, F., Berger, A., and Loutre, M.-F. (1996). Alternate interpretation of the Messinian salinity crisis: controversy resolved? *Geology*, 24(4), 363–366.
- Cowie, P. A., Whittaker, A. C., Attal, M., Roberts, G., Tucker, G. E., and Ganas, A. (2008). New constraints on sediment-flux-dependent river incision: Implications for extracting tectonic signals from river profiles. *Geology*, 36(7), 535–538.
- Crosby, B. T. and Whipple, K. X. (2006). Knickpoint initiation and distribution within fluvial networks: 236 waterfalls in the Waipaoa River, North Island, New Zealand. *Geomorphology*, 82, 16–38.
- Daniels, J. M. (2008). Distinguishing allogenic from autogenic causes of bed elevation change in late Quaternary alluvial stratigraphic records. *Geomorphology*, 101, 159–171.
- Dubar, M. (1984). Chronologie et signification des dépôts continentaux du Néogène supérieur du bassin de Riez-Valensole (Alpes-de-Haute-Provence, France). *Bull. Soc. Géol. Fr.*, 7(5), 971–978.
- Dubar, M., Aguilar, J.-P., Chaline, J., Michaux, J., and Semah, F. (1998). Données chronologiques (mammifères et magnétostratigraphie) sur les dépôts plio-pleistocènes au toit du bassin de Valensole; implications morphodynamiques. *Géol. Fr.*, 1, 57–68.
- Dubar, M., Guerin, C., and Heintz, E. (1978). Les nouveaux gisements villafranchiens du ravin de Cornillet (Moustiers Sainte-Marie, Alpes de Haute Provence, France) et leur contexte géologique. *Geobios*, 11(3), 367–381.
- Ely, L. L. (1997). Response of extreme floods in the southwestern United States to climatic variations in the late Holocene. *Geomorphology*, 19, 175–201.
- Espurt, N., Hippolyte, J.-C., Saillard, M., and Bellier, O. (2012). Geometry and kinematic evolution of a long-living foreland structure inferred from field data and cross section balancing, the Sainte-Victoire System, Provence, France. *Tectonics*, 31(4), article no. TC4021.
- Fabre, G. and Nicod, J. (1978). Niveaux de base actuels dans les principaux canyons du Languedoc oriental et des Plans de provence. *Int. J. Speleol.*, 10(3), 279–291.
- Ford, M. and Lickorish, W. H. (2004). Foreland basin evolution around the western Alpine Arc. Geological Society, London, Special Publications, 221(1), pages 39–63. Geological Society of London.
- Ford, M., Lickorish, W. H., and Kusznir, N. J. (1999). Tertiary foreland sedimentation in the Southern Subalpine Chains, SE France: a geodynamic appraisal. *Basin Res.*, 11(4), 315–336.
- Glotzbach, C., van der Beek, P. A., and Spiegel, C. (2011). Episodic exhumation and relief growth in the Mont Blanc massif, Western Alps from numerical modelling of thermochronology data. *Earth Planet. Sci. Lett.*, 304(3–4), 417–430.

- Godard, V., Hippolyte, J.-C., Cushing, E., Espurt, N., Fleury, J., Bellier, O., et al. (2020). Hillslope denudation and morphologic response to a rock uplift gradient. *Earth Surf. Dyn.*, 8(2), 221–243.
- Goguel, J. (1935). La formation du réseau hydrographique du Verdon. *Ann. Géogr.*, 44, 492–495.
- Guerit, L., Dominguez, S., Malavieille, J., and Castellort, S. (2016). Deformation of an experimental drainage network in oblique collision. *Tectonophysics*, 693, 210–222.
- Hartshorn, K., Hovius, N., Dade, W. B., and Slingerland, R. L. (2002). Climate-Driven Bedrock Incision in an Active Mountain Belt. *Science*, 297(5589), 2036–2038.
- Haug, G. H., Ganopolski, A., Sigman, D. N., Rosell-Mele, A., Swann, G. E. A., Tiedemann, R., et al. (2005). North Pacific seasonality and the glaciation of North America 2.7 million years ago. *Nature*, 433, 821–825.
- Herman, E., Seward, D., Valla, P. G., Carter, A., Kohn, B., Willett, S. D., and Ehlers, T. A. (2013). Worldwide acceleration of mountain erosion under a cooling climate. *Nature*, 504(7480), 423–426.
- Hippolyte, J.-C., Clauzon, G., and Suc, J.-P. (2011). Messinian-Zanclean canyons in the Digne nappe (southwestern Alps): tectonic implications. *Bull. Soc. Géol. Fr.*, 182(2), 111–132.
- Hippolyte, J.-C. and Dumont, T. (2000). Identification of Quaternary thrusts, folds and faults in a low seismicity area: examples in the Southern Alps (France). *Terra Nova*, 12(4), 156–162.
- Howard, A. D., Dietrich, W. E., and Seidl, M. A. (1994). Modeling fluvial erosion on regional to continental scales. *J. Geophys. Res. Solid Earth*, 99(B7), 13971–13986.
- Jansen, J. D., Codilean, A. T., Bishop, P., and Hoey, T. B. (2010). Scale dependence of lithological control on topography: Bedrock channel geometry and catchment morphometry in Western Scotland. *J. Geol.*, 118(3), 223–246.
- Jansen, J. D., Fabel, D., Bishop, P., Xu, S., Schnabel, C., and Codilean, A. T. (2011). Does decreasing paraglacial sediment supply slow knickpoint retreat? *Geology*, 39(6), 543–546.
- Johnson, J. P. L., Whipple, K. X., and Sklar, L. S. (2010). Contrasting bedrock incision rates from snowmelt and flash floods in the Henry Mountains, Utah. *Geol. Soc. Am. Bull.*, 122(9–10), 1600–1615.
- Jorda, M. (1975). Les montagnes du Haut Verdon, Etude géomorphologique. *Méditerranée*, 20(1), 37–58.
- Jourdon, A., Rolland, Y., Petit, C., and Bellahsen, N. (2014). Style of Alpine tectonic deformation in the Castellane fold-and-thrust belt (SW Alps, France): Insights from balanced cross-sections. *Tectonophysics*, 633, 143–155.
- Lague, D., Hovius, N., and Davy, P. (2005). Discharge, discharge variability, and the bedrock channel profile. *J. Geophys. Res. Earth Surf.*, 110(F4), article no. F04006.
- Larroque, C., Baise, S., Albaric, J., Jomard, H., et al. (2021). Seismotectonic of southeast France: from Jura mountains to Corsica. *C. R. Géosci.*, 353(S1), 105–151.
- Le Pichon, X., Rangin, C., Hamon, Y., Loget, N., Lin, J. Y., Andreani, L., and Flotte, N. (2010). Geodynamics of the France Southeast Basin. *Bull. Soc. Géol. Fr.*, 6, 477–501.
- Lisiecki, L. E. (2010). Links between eccentricity forcing and the 100,000-year glacial cycle. *Nat. Geosci.*, 3, 349–352.
- Martel, E.-A. (1908). Le profil en long du Grand Cañon du Verdon. *Ann. Géogr.*, 17, 395–403.
- Molnar, P. (2007). Climate change, flooding in arid environments, and erosion rate. *Geology*, 29, 1071–1074.
- Muttoni, G., Carcano, C., Garzanti, E., Ghielmi, M., Piccin, A., Pini, R., et al. (2003). Onset of major Pleistocene glaciations in the Alps. *Geology*, 31(11), 989–992.
- Nicod, J. (2004). Présentation du bloc-diagramme: Grand Canyon du Verdon. *Méditerranée*, 102(1), 17–24.
- Nouibat, A., Stehly, L., Paul, A., Schwartz, S., Bodin, T., Dumont, T., et al. (2022). Lithospheric transdimensional ambient-noise tomography of W-Europe: implications for crustal-scale geometry of the W-Alps. *Geophys. J. Int.*, 229(2), 862–879.
- Oberlander, T. M. (1965). *The Zagros Streams: A New Interpretation of Transverse Drainage in an Orogenic Zone*. Syracuse Geographical Series, 1. Syracuse University Press, Syracuse.
- Ouimet, W. B., Whipple, K. X., Crosby, B. T., Johnson, J. P., and Schildgen, T. F. (2008). Epigenetic gorges in fluvial landscapes. *Earth Surf. Process. Landsc.*, 33, 1993–2009.
- Petit, C., Rolland, Y., Braucher, R., Bourlès, D., Guilou, V., and Petitperrin, V. (2019). River incision and

- migration deduced from  $^{36}\text{Cl}$  cosmic-ray exposure durations: The Clue de la Cerise gorge in southern French Alps. *Geomorphology*, 330, 81–88.
- Piña Valdés, J., Socquet, A., Beauval, C., Doin, M.-P., D'Agostino, N., and Shen, Z.-K. (2022). 3D GNSS velocity field sheds light on the deformation mechanisms in Europe: Effects of the vertical crustal motion on the distribution of seismicity. *J. Geophys. Res. Solid Earth*, 127, article no. e2021JB023451.
- Rolland, Y., Darnault, R., Braucher, R., Bourlès, R., Petit, C., Bouissou, S., and ASTER Team (2019). Deglaciation history at the Alpine-Mediterranean transition (Argentera-Mercantour, SW Alps) from  $^{10}\text{Be}$  dating of moraines and glacially polished bedrock. *Earth Surf. Process. Landsf.*, 45(2), 393–410.
- Rolland, Y., Petit, C., Saillard, M., Braucher, R., Bourlès, D., Darnault, R., et al. (2017). Inner gorges incision history: A proxy for deglaciation? Insights from Cosmic Ray Exposure dating ( $^{10}\text{Be}$  and  $^{36}\text{Cl}$ ) of river-polished surfaces (Tinée River, SW Alps, France). *Earth Planet. Sci. Lett.*, 457, 271–281.
- Saillard, M., Petit, C., Rolland, Y., Braucher, R., Bourlès, D. L., Zerathe, S., Revel, M., and Jourdon, A. (2014). Late Quaternary incision rates in the Vésubie catchment area (Southern French Alps) from in situ-produced  $^{36}\text{Cl}$  cosmogenic nuclide dating: Tectonic and climatic implications. *J. Geophys. Res. Earth Surf.*, 119, 1121–1135.
- Sanchez, G., Rolland, Y., Schreiber, D., Giannerini, G., Corsini, M., and Lardeaux, J. M. (2010). The active fault system of SW Alps. *J. Geodyn.*, 49(5), 296–302.
- Schaller, M., Hovius, N., Willett, S. D., Ivy-Ochs, S., Snyal, H.-A., and Chen, M.-C. (2005). Fluvial bedrock incision in the active mountain belt of Taiwan from in situ-produced cosmogenic nuclides. *Earth Surf. Process. Landsf.*, 30, 955–971.
- Schimmelpfennig, I., Benedetti, L., Finkel, R., Pik, R., Blard, P.-H., Bourlès, D. L., Burnard, P., and Williams, A. (2009). Source of in situ  $^{36}\text{Cl}$  in basaltic rocks. Implication for calibration of production rates. *Quat. Geochronol.*, 4, 441–461.
- Schumm, S. A. (1977). *The Fluvial System*. Wiley, New York.
- Schwartz, S., Gautheron, C., Audin, L., Dumont, T., Nomade, J., Barbarand, J., et al. (2017). Foreland exhumation controlled by crustal thickening in the Western Alps. *Geology*, 45(2), 139–142.
- Siame, L., Bellier, O., Braucher, R., Sébrier, M., Cushing, M., Bourlès, D., et al. (2004). Local erosion rates versus active tectonics: Cosmic ray exposure modelling in Provence (south-east France). *Earth Planet. Sci. Lett.*, 220(3–4), 345–364.
- Sklar, L. S. and Dietrich, W. E. (2001). Sediment and rock strength controls on river incision into bedrock. *Geology*, 29(12), 1087–1090.
- Sklar, L. S. and Dietrich, W. E. (2006). The role of sediment in controlling steady-state bedrock channel slope: Implications of the saltation–abrasion incision model. *Geomorphology*, 82, 58–83.
- Sternai, P., Sue, C., Husson, L., Serpelloni, E., Becker, T. W., Willett, S. D., et al. (2019). Present-day uplift of the European Alps: Evaluating mechanisms and models of their relative contributions. *Earth Sci. Rev.*, 190, 589–604.
- Stokes, M., Mather, A. E., Belfoul, A., and Farik, F. (2008). Active and passive tectonic controls for transverse drainage and river gorge development in a collisional mountain belt (Dades Gorges, High Atlas Mountains, Morocco). *Geomorphology*, 102(1), 2–20.
- Stone, J. O. (2000). Air pressure and cosmogenic isotope production. *J. Geophys. Res. Solid Earth*, 105, 23753–23759.
- Suc, J.-P. and Zagwijn, W. H. (1983). Plio-Pleistocene correlations between the northwestern Mediterranean region and northwestern Europe according to recent biostratigraphic and palaeoclimatic data. *Boreas*, 12(3), 153–166.
- Twidale, C. R. (2004). River patterns and their meaning. *Earth Sci. Rev.*, 67(3–4), 159–218.
- Valla, P. G., Shuster, D. L., and van der Beek, P. A. (2011). Significant increase in relief of the European Alps during mid-Pleistocene glaciations. *Nat. Geosci.*, 4(10), 688–692.
- Valla, P. G., van der Beek, P. A., and Carcaillet, J. (2010). Dating bedrock gorge incision in the French Western Alps (Ecrin-Pelvoux massif) using cosmogenic  $^{10}\text{Be}$ . *Terra Nova*, 22, 18–25.
- Whipple, K. X. (2004). Bedrock rivers and the geomorphology of active orogens. *Annu. Rev. Earth Planet. Sci.*, 32(1), 151–185.
- Whipple, K. X., Hancock, G. S., and Anderson, R. S. (2000). River incision into bedrock: Mechanics and relative efficacy of plucking, abrasion, and cavitation. *Geol. Soc. Am. Bull.*, 112(3), 490–503.



- Whipple, K. X. and Tucker, G. E. (1999). Dynamics of the stream-power river incision model: Implications for height limits of mountain ranges, landscape response timescales, and research needs. *J. Geophys. Res. Solid Earth*, 104(B8), 17661–17674.
- Wobus, C., Whipple, K. X., Kirby, E., Snyder, N., Johnson, J., Spyropolou, K., et al. (2006). Tectonics from topography: Procedures, promise, and pitfalls. In *Tectonics, Climate, and Landscape Evolution*, Special Papers-Geological Society of America, 398, page 55. Geological Society of America.
- Zerathe, S., Lebourg, T., Braucher, R., and Bourlès, D. (2014). Mid-Holocene cluster of larger-scale landslides revealed in the Southwestern Alps by  $^{36}\text{Cl}$  dating. Insight on an Alpine-Scale landslide activity. *Quat. Sci. Rev.*, 90, 106–127.